Space-Charge-Limited Current in a Film

ANATOLY A. GRINBERG, SERGE LURYI, FELLOW, IEEE, MARK R. PINTO, AND NORMAN L. SCHRYER

Abstract—**We consider the space-charge-limited current in a thin-film n-i-n diode. It is assumed that "impenetrable" barriers limit the current flow to a film of thickness *D*. Because the electric field of injected electrons spreads out of the film, the level of injection is substantially higher than in the bulk case described by the classical Mott-Gurney law. As a consequence, the current density in a thin diode can be an order of magnitude larger than in a bulk diode of the same length. It is shown that, in the limit of small *D*, the total current is independent of *D* because the decreasing film thickness is exactly compensated by increasing injection. In this limit, we have obtained analytic expressions of the current-voltage characteristics for several model electrode configurations. The analytic results are confirmed by a numerical simulation of the diode within a drift-diffusion model assuming a field-independent mobility. Our numerical results also describe a transition with decreasing *D* from the Mott-Gurney law to the law governing space-charge-limited current in a film.**

I. Introduction

SPACE-CHARGE-LIMITED (SCL) current in a bulk double-injection n-i-n diode has been studied in a number of papers beginning with the classical work by Mott and Gurney [1]. Conduction in such structures is due to electrons injected into the (i) base. The uncompensated charge of injected electrons limits the current. In the present work, we shall consider the SCL current in a thin-film diode. It will be assumed that potential barriers confine the current flow within a semiconductor layer of thickness D. Such a problem was first considered by Geurst [2] in the limit $D \to 0$ and for a special contact geometry. On the basis of this analysis Geurst was able to construct [3] an analytic model of an FET, which goes beyond the usual gradual channel approximation.

One can say that the SCL current in a film corresponds to the limit that in some sense is precisely opposite to the gradual channel approximation. Indeed, the latter approximation, introduced by Shockley, corresponds to the assumption that the channel charge is induced by the gate while the source-to-drain current affects the carrier concentration at a given point in the channel only by changing the local electrostatic potential relative to the gate. On the other hand, the mobile charge, carrying an SCL current, is induced by the drain electrode—closely resembling the situation in the pinchoff region of an FET channel. Our present approach to the problem of SCL current is quite different methodologically from that used earlier [2]. It yields a unified analytical description for several different diode geometries and gives us grounds to believe that a similar approach can be used to describe the SCL current in transistors.

Strictly speaking, in an n-i-n structure—whether one deals with the bulk or the film case—the mechanism of electron transport is different in different parts of the diode. In a symmetrical structure at equilibrium the electric field E_x vanishes in the middle of the diode base. As an external bias V is applied, the point where $E_x = 0$ moves toward the cathode. This point defines the position of the so-called "virtual cathode." In the bulk case, the virtual cathode geometry is obvious: it represents a plane perpendicular to the current flow. Only the position of this plane changes with an applied bias. For a film, the virtual cathode represents a surface defined by the condition of vanishing *normal component* of the field. This surface is not necessarily an equipotential and its exact shape cannot be determined without considering the diffusion current component. The usefulness of the virtual cathode concept lies in the fact that it allows separation of the mobile charge in the base into two groups: for charges located on the anode side of the virtual cathode surface the electric field lines terminate on the positive charge at the anode electrode, whereas for charges located on the cathode side of the surface the field lines terminate on the cathode electrode.

The transport of electrons between the cathode contact and the virtual cathode cannot be described without accounting for diffusion because in this region electrons move against the electric field. However, with increasing bias this region shrinks, and for a sufficiently high V almost the entire base of the diode is located between the virtual cathode and the anode where the dominant transport mechanism is carrier drift in the electric field.

The virtual-cathode *approximation* corresponds to neglecting the variation of the quasi-Fermi level on the cathode side of the virtual cathode and the diffusion transport on the anode side. In this approximation the entire injected charge has field lines terminating on the anode. It has been rigorously shown [4] that in a bulk diode the virtual cathode approximation is quite accurate, provided $V \gtrsim 10kT/e$. In the present work, we shall be mainly interested in the large-current limit, where this approximation is certainly justified. Our results will be confirmed by a numerical simulation that does not rely on the virtual cathode approximation and can be regarded as an exact solution of a drift-diffusion model.

Manuscript received November 10, 1988; revised February 15, 1989. The review of this paper was arranged by Associate Editor R. P. Jindal.
The authors are with AT&T Bell Laboratories, Murray Hill, NJ 07974.
IEEE Log Number 8927643.

0018-9383/89/0600-1162$01.00 © 1989 IEEE

The general form of the law governing SCL current in the virtual-cathode approximation can be obtained from a simple dimensionality argument. Indeed, in CGS units conductivity has the dimensionality of a velocity. Taking this velocity to be an effective carrier velocity v, we can write a generic expression for the SCL current in the form

$$I \propto \frac{\epsilon}{4\pi} vV \frac{A}{L^2} \quad \text{(bulk)}$$

$$I \propto \frac{\epsilon}{4\pi} vV \frac{W}{L} \quad \text{(film)} \qquad (1)$$

where L is the length, $A = D \cdot W$ the cross-sectional area, and W the width of the diode; cf. Fig. 1. The relative permittivity ϵ of the material, dimensionless in CGS units, enters because it scales the space-charge potential in Poisson's equation. The actual current-voltage dependence (up to a numerical coefficient) can be "derived" from (1) whenever the conduction process involves a dominant transport mechanism, which provides a unique scaling relationship between v and V. Thus, for a free electron motion, the velocity scales as $v^2 \propto (e/m)V$ and one obtains laws appropriate for ballistic transport, e.g., for the bulk case Child's law [5] $I \propto (\epsilon/4\pi)(e/m)^{1/2}V^{3/2}(A/L^2)$. For the case when electron velocity is saturated, the law is of the form (1) with $v = v_{sat}$, and for the case of constant mobility μ, the velocity scales as $v \propto \mu V/L$ leading to the following expressions:

$$I = \zeta_3 \frac{\epsilon}{4\pi} \frac{\mu V^2}{L^3} A \quad \text{(bulk)}$$

$$I = \zeta_2 \frac{\epsilon}{4\pi} \frac{\mu V^2}{L^2} W \quad \text{(film)}. \qquad (2)$$

The numerical coefficient ζ_3 corresponding to the bulk case equals $\zeta_3 = 9/8$, as first calculated by Mott and Gurney. For the case of a film, the corresponding coefficient ζ_2 is not universal but depends on the shape of the contacts, as will be shown below.

In this work we have analyzed three representative geometries, illustrated in Fig. 1(a)-(c). These are: (a) edge (line) contacts, (b) contacts in the form of two semi-infinite strips that have the same thickness as the film (this geometry is similar to that studied by Geurst [2]), and (c) contacts in the form of two infinite planes perpendicular to the film. We have evaluated ζ_2 (in the limit $D \to 0$) for each of these geometries (Sections III-A to III-C). The results are compared (Section IV) against numerical solutions obtained for each geometry with the help of the drift-diffusion device simulator PADRE.[1] These solutions also describe the transition between the bulk and the film SCL current regimes with decreasing D.

[1]M. R. Pinto and R. K. Smith, "PADRE," AT&T Bell Labs. Internal Rep. PADRE is a successor to the PISCES device simulator; see M. R. Pinto, C. S. Rafferty, and R. W. Dutton, "PISCES-II: Poisson and continuity equation solver," Stanford Electron. Lab. Tech. Rep., Stanford Univ., 1984.

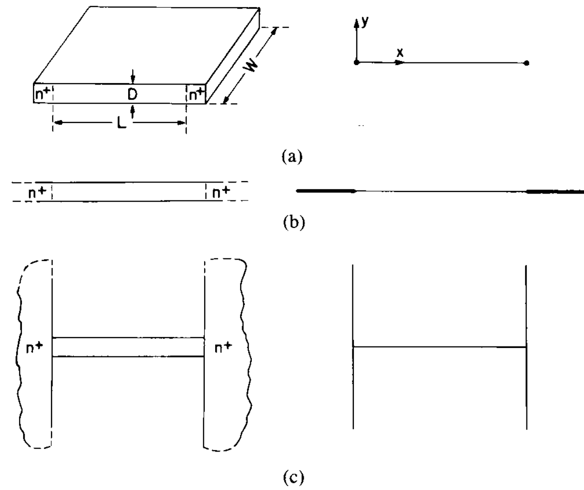

Fig. 1. Illustration of thin-film contact geometries considered in this work. The conducting contacts are provided by heavily doped semiconductor regions. The film lies in the xy plane. (a) "Edge contacts": Cross section of the contact is a square with the side equal to film thickness D. In the limit $D \to 0$, the contact is modeled by conducting filament. (b) "Strip contacts": The contacts are doped layers of the same thickness as the thin-film base. In the limit $D \to 0$, the contacts are model as conducting planes co-planar to the base. (c) "H-shaped contacts": The contacts represent doped bulk regions, modeled as conducting planes perpendicular to the plane of the base.

Our method of solution is as follows: first we find the Green function of the Poisson equation describing the electric field of the injected charge and the charge induced on the electrodes. For *edge* contacts (Fig. 1(a)), the location of charge on the anode electrode is specified and evaluation of the two-dimensional potential distribution is straightforward. For *extended* contacts (Fig. 2(b), (c)) the induced charge is distributed in a non-trivial way, and the easiest way to include it is to use a Green function, satisfying the boundary condition of a fixed potential on the conducting electrode surfaces. The total potential and field distribution in the device is found next by integrating over the injected charge density. The latter is locally related to the current and the total local electric field—including that due to external charges on the electrodes. This procedure leads to a nonlinear integral equation for the injected charge density, which we solve numerically as well as analytically (with the help of an accurate approximation). Once the charge distribution is known, the SCL current–voltage characteristic is readily determined. The procedure is first illustrated in Section II for the case of a bulk diode, where it is used to derive the classical Mott–Gurney law, and then applied in the subsequent sections to thin-film cases with different electrode geometries.

Most of our results are derived in the approximation of constant mobility. However, we have also considered the SCL current in the opposite limit, corresponding to a vanishing differential mobility and constant "saturated" velocity $v = v_{sat}$. An exact expression for the current-voltage characteristic in this limit, presented in Section III-B for the strip-contact geometry (Fig. 1(b)), allows us to assess the range of validity of the constant-mobility ap-

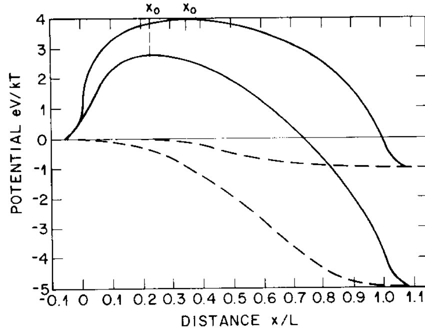

Fig. 2. Energy-band diagram of bulk n-i-n diode under a small applied bias V (after [4]). The dashed line shows the quasi-Fermi level, and x_0 indicates the position of the virtual cathode plane, which rapidly moves toward the real cathode as the bias increases.

proximation and to illustrate the effect of velocity saturation.[2]

II. Illustration of the Solution Method in the Instance of a Bulk Diode

Fig. 2 shows the conduction-band diagram and the quasi-Fermi level variation in a bulk n-i-n diode under a small applied bias [4]. In the virtual cathode approximation, the charge density in the base ($0 \le x \le L$) can be written in the form

$$\rho(x) = -en(x) + eP\delta(L - x) \tag{3}$$

where

$$P \equiv \int_0^L n(x)\,dx. \tag{4}$$

In writing ρ in the form of (3), we neglected the separation of the virtual cathode from the cathode (setting $x_0 = 0$) and placed at the plane $x = L$ all the positive anode charge neutralizing the charge $n(x)$, injected into the region between the virtual cathode and the anode. The charge density ρ obeys the total neutrality condition.

The electrostatic potential in the diode base is determined by the Poisson equation

$$\frac{d^2\phi}{dx^2} = -\frac{4\pi}{\epsilon}\rho(x) \tag{5}$$

and the boundary conditions

$$\frac{d\phi}{dx} = 0, \quad \text{at } x \equiv x_0 = 0 \tag{6a}$$

$$\phi(L) = V. \tag{6b}$$

The Green function $G(x, x') = -(1/2)|x - x'|$ of the Poisson equation (5) allows to write its solution in the form

$$\phi(x) = -\frac{2\pi}{\epsilon}\int_0^L |x - x'|\rho(x')\,dx' = \frac{2\pi e}{\epsilon}\int_0^L [|x - x'| + |L - x|]n(x')\,dx'. \tag{7}$$

Note that the charge density ρ chosen as in (3) to satisfy total neutrality automatically guarantees that the boundary condition (6a) is obeyed, as it follows from Gauss' law and also can be seen from the expression for the electric field in the base, obtained from (7)

$$E(x) = -\frac{d\phi}{dx} = -\frac{4\pi e}{\epsilon}\int_0^x n(x')\,dx'. \tag{8}$$

Equation (8) combined with the constant-mobility approximation for the current density

$$j = e\mu n(x)\,E(x) \tag{9}$$

leads to the following nonlinear integral equation for the carrier density:

$$\frac{4\pi e^2\mu}{-\epsilon j}\,n(x)\int_0^x n(x')\,dx' = 1 \tag{10}$$

and the solution of this equation is of the form

$$n(x) = \left(-\frac{\epsilon j}{8\pi e^2\mu x}\right)^{1/2}. \tag{11}$$

When substituted in (7) and using (6b), this solution yields the Mott–Gurney law

$$I = -\frac{9\mu}{8}\frac{\epsilon}{4\pi}\frac{V^2}{L^3}A. \tag{12}$$

The method employed in the above derivation of the Mott–Gurney law is somewhat different from that used before [1], [4] and has the advantage of being convenient to generalize to the case of a thin film.

III. SCL Current in Thin Films: Analytical Results

Our analytic treatment will be confined to the limiting case of a vanishing film thickness. Physically, it is sufficient to assume that $D \ll L$. Instead of the current density (9) we shall be using a linear current density

$$J \equiv I/W = e\mu n_s(x)\,E_x(x) \tag{13}$$

where n_s is the surface electron concentration in the film and E_x is the x component of the electric field in the film ($y = 0$). The potential distribution in the device, now determined by the two-dimensional Poisson equation

$$\frac{d^2\phi}{dx^2} + \frac{d^2\phi}{dy^2} = -\frac{4\pi}{\epsilon}\rho(x) \tag{14}$$

must satisfy the boundary conditions on the electrodes and be consistent with (13).

[2] Space-charge-limited currents in *bulk* materials with nonlinear velocity-field relationships have been considered by G. Sh. Gildenblat, A. R. Rao, and S. S. Cohen, *IEEE Trans. Electron Devices*, vol. ED-34, p. 2165, 1987. Exact solutions obtained by these authors describe the gradual transition from the constant-mobility and the saturated-velocity regimes for several v–E models.

A. Film with Edge Contacts

The contact geometry is illustrated in Fig. 1(a). In this simplest case, there are no extended electrodes, and consequently the charge density can be written in the form

$$\rho(x, y) = e\delta(y)[-n_s(x) + P_s\delta(L - x)] \quad (15)$$

where

$$P_s \equiv \int_0^L n_s(x)\, dx.$$

The solution then almost exactly parallels that presented in Section II for the bulk diode. Using the Green function of the Poisson equation (14)

$$G(x - x', y - y') = -\frac{1}{2\pi} \ln\left[(x - x')^2 + (y - y')^2\right]^{1/2} \quad (16)$$

corresponding to a filament source, the x component of the electric field in the film can be found readily

$$E_x(x, 0) = -\frac{2e}{\epsilon(L - x)} \int_0^L \frac{(L - x')}{(x - x')} n_s(x')\, dx'. \quad (17)$$

Substituting E_x into (13), we obtain a nonlinear integral equation for $n_s(x)$

$$\frac{n_s(x)}{(L - x)} \int_0^L n_s(x') \frac{(L - x')}{(x - x')} dx' = -\frac{J\epsilon}{2e^2\mu}. \quad (18)$$

Introducing dimensionless variables

$$\xi \equiv \frac{x}{L}$$
$$\nu_s(\xi) = \left(\frac{2e^2\mu}{-J\epsilon}\right)^{1/2} n_s(\xi) \quad (19)$$

we can rewrite (18) in the form

$$\frac{\nu_s(\xi)}{(1 - \xi)} \int_0^1 \frac{(1 - \xi')}{(\xi - \xi')} \nu_s(\xi')\, d\xi' = 1. \quad (20)$$

An approximate solution of this equation can be represented in the form

$$\nu_s(\xi) = a\xi^\alpha(1 - \xi)^{1/2} \quad (21)$$

with $a \approx 0.5$ and $\alpha \approx -0.36$. As shown in the Appendix, this analytic approximation gives excellent agreement with the numerical solution. Using (13) and (19), the applied voltage can be written in the form

$$V = -\int_0^L E_x(x, 0)\, dx = \left(\frac{-2JL^2}{\epsilon\mu}\right)^{1/2} \int_0^1 \frac{d\xi}{\nu_s(\xi)}. \quad (22)$$

From the approximate solution (21), the last integral equals

$$\int_0^1 \frac{d\xi}{\nu_s(\xi)} = \frac{\pi^{1/2}\Gamma(1 - \alpha)}{a\Gamma(\frac{3}{2} - \alpha)} \approx 2.35$$

whence the current–voltage characteristic is given by

$$J = -0.57 \frac{\epsilon}{4\pi} \frac{\mu V^2}{L^2}. \quad (23)$$

We see that the characteristic is of the form (2) with $\zeta_2^a \approx 0.57$.

B. Film with Two Coplanar Strip Contacts

This is the geometry considered by Geurst [2]. It is somewhat more complicated than that considered in Section III-A because we do not know *a priori* the charge distribution induced in the extended contacts. We can circumvent this problem by using the Green function of Poisson's equation (14) *subject* to the boundary condition that *both* electrodes are at *zero* potential. Potential $\tilde{\phi}(x, y)$ determined with the help of this function must then be added to the potential determined from the homogeneous (Laplace) equation corresponding to electrodes biased by V and no mobile charge.

The Green function $G(x, x'; y, y')$ can be found by the standard methods of conformal mapping [6], using the method of images for the source charge. For our purposes, we need only the values of $G(x, x'; y, y')$ at $y = y' = 0$. This function is of the form

$$G(\xi, \xi') = \frac{1}{2\pi} \operatorname{Re} \ln \left(\frac{\sin[(\psi + \psi')/2]}{\sin[(\psi - \psi')/2]}\right) \quad (24)$$

where

$$\xi \equiv \frac{2x - L}{L}, \qquad \psi \equiv \arccos(\xi)$$
$$\xi' \equiv \frac{2x' - L}{L}, \qquad \psi' \equiv \arccos(\xi').$$

From this function the potential produced by injected electrons is obtained in the following form:

$$\tilde{\phi}(\xi) = -\frac{2\pi eL}{\epsilon} \int_{-1}^{+1} n_s(\xi')\, G(\xi, \xi')\, dx' \quad (25)$$

and the total potential is given by[1]

$$\phi(\xi) = \tilde{\phi}(\xi) + V[1 - \psi(\xi)/\pi]. \quad (26)$$

Differentiating (26), we find the electric field distribution in the film

$$E_x(\xi) \equiv -\frac{2}{L}\frac{\partial\phi}{\partial\xi} = \frac{-2}{(1 - \xi^2)^{1/2}} \cdot \left(\frac{e}{\epsilon} \int_{-1}^{1} \frac{n_s(\xi')(1 - \xi'^2)^{1/2}\, d\xi'}{(\xi - \xi')} + \frac{V}{\pi L}\right). \quad (27)$$

Expressing E_x with the help of (13) in terms of the surface concentration n_s and writing V in the form similar to (22),

$$V = \left(\frac{-JL^2}{2\epsilon\mu}\right)^{1/2} \int_0^1 \frac{d\xi}{\nu_s(\xi)} \quad (28)$$

where ν_s is the dimensionless surface concentration defined in (19), we bring (27) into the form of a nonlinear integral equation for ν_s

$$\int_{-1}^{1}\left(\frac{1}{\pi\nu_s(\xi')}+\frac{\nu_s(\xi')(1-\xi'^2)^{1/2}}{\xi-\xi'}\right)d\xi' = \frac{(1-\xi^2)^{1/2}}{\nu_s(\xi)}. \tag{29}$$

An accurate approximation for the solution of this equation is achieved by taking ν_s in the form

$$\nu_s(\xi) = a(1+\xi)^{\alpha}(1-\xi)^{\beta} \tag{30}$$

with $a^2 \approx 0.18$, $\alpha \approx -0.4$, and $\beta \approx 0.4$. When substituted in (28), this yields a current-voltage characteristic of the form of (2) with

$$\zeta_2^b \approx \frac{2^{1+2\alpha+2\beta}\pi a^2[\Gamma(2-\alpha-\beta)]^2}{[\Gamma(1-\alpha)\Gamma(1-\beta)]^2} \approx 0.70. \tag{31}$$

The result obtained by Geurst [2] for this case corresponds to $\zeta_2^b = 2/\pi \approx 0.64$.

It is interesting to compare these results, obtained under the assumption of a constant mobility with the opposite limiting case, when the differential mobility is zero and the carrier velocity is saturated, $v = v_{\text{sat}}$. In this case, the carrier concentration is uniquely determined by the current density—independently of the local electric field—and is uniform

$$n_s = -\frac{J}{ev_{\text{sat}}}. \tag{32}$$

Substituting (32) into (27) and integrating, we find the electric field

$$E_s(\xi) = -\frac{2}{(1-\xi^2)^{1/2}}\left(\frac{\pi\xi J}{\epsilon v_{\text{sat}}} - \frac{V}{\pi L}\right). \tag{33}$$

The field must vanish at the virtual cathode position, $x = 0$, i.e. $E_x(\xi = -1) = 0$, whence

$$J = -\frac{\epsilon}{4\pi}\frac{4v_{\text{sat}}V}{\pi L}. \tag{34}$$

The law (34) gives the correct expression for the SCL current in the high-bias limit. Note that it corresponds to a different scaling of the current with the diode length (L^{-1} instead of L^{-2}).

Whenever the law (2) predicts a higher current than (34), it is a clear indication that the constant-mobility approximation is invalid. For the strip-contact geometry this happens when V exceeds the value

$$\frac{4}{\pi\zeta_2^b}\frac{v_{\text{sat}}L}{\mu}.$$

C. Film with Two Perpendicular Plane Contacts

The electrode geometry under consideration in this section is illustrated in Fig. 1(c). Green's function of the Poisson equation (14) subject to the boundary condition of zero potential on both conducting planar electrodes is given by [7]

$$G(x, x'; y, y') = \frac{1}{2\pi}\tanh^{-1} \cdot \left(\frac{\sin(\pi\xi)\sin(\pi\xi')}{\cosh[\pi(\eta-\eta')] - \cos(\pi\xi)\cos(\pi\xi')}\right) \tag{35}$$

where $\xi \equiv x/L$, $\xi' \equiv x'/L$, $\eta \equiv y/L$, and $\eta' \equiv y'/L$. With the volume density of injected electrons in the film given by

$$n(x, y) = n_s(x)\,\delta(y) \tag{36}$$

where n_s is the surface electron density, the Green function (35) leads to a potential function $\tilde{\phi}$ of the form

$$\begin{aligned}\tilde{\phi}(\xi,\eta) &= -\frac{4\pi eL^2}{\epsilon}\iint n(\xi',\eta') \cdot G(\xi,\xi';\eta-\eta')\,d\xi'\,d\eta' \\ &= -\frac{2eL}{\epsilon}\int_0^1 n_s(\xi')\tanh^{-1} \cdot \left(\frac{\sin(\pi\xi)\sin(\pi\xi')}{\cosh(\pi\eta) - \cos(\pi\xi)\cos(\pi\xi')}\right)d\xi'.\end{aligned} \tag{37}$$

This potential function corresponds to a source consisting of the injected charge n_s and the charges induced by n_s on the electrodes—but not the charges induced by the biased electrodes on one another. The corresponding portion of the electric field equals

$$\tilde{E}_x(\xi,\eta) = \frac{2\pi e}{\epsilon}\int_0^1 n_s(\xi')\frac{[\cos(\pi\xi)\cosh(\pi\eta) - \cos(\pi\xi')]\sin(\pi\xi')}{[\cosh(\pi\eta) - \cos(\pi\xi)\cos(\pi\xi')]^2 - [\sin(\pi\xi)\sin(\pi\xi')]^2}\,d\xi'. \tag{38}$$

Note that $(\epsilon/4\pi)\tilde{E}_x(0,\eta)$ and $(\epsilon/4\pi)\tilde{E}_x(L,\eta)$ give the density of charge induced by n_s on the cathode and the anode electrodes, respectively. The total charges induced by n_s on the contact plates are given by

$$\begin{aligned}Q(0) &= \frac{\epsilon L}{4\pi}\int_{-\infty}^{+\infty}\tilde{E}_x(0,\eta)\,d\eta = eL\int_0^1(1-\xi)n_s(\xi)\,d\xi \\ Q(L) &= -\frac{\epsilon L}{4\pi}\int_{-\infty}^{+\infty}\tilde{E}_x(L,\eta)\,d\eta = eL\int_0^1 \xi n_s(\xi)\,d\xi.\end{aligned} \tag{39}$$

Both induced charges are positive, and their sum equals the total charge of electrons injected in the film.

The *total* electric field and electrostatic potential are

given by

$$E_x(\xi, \eta) = \tilde{E}_x(\xi, \eta) - \frac{V}{L} \quad (40)$$

$$\phi(\xi, \eta) = \tilde{\phi}(\xi, \eta) + V\xi. \quad (41)$$

The field $\tilde{E}_x$ in the plane of the film is determined from (38) and equals

$$\tilde{E}_x(\xi, 0) = \frac{2\pi e}{\epsilon} \int_0^1 \frac{n_s(\xi') \sin(\pi\xi')\, d\xi'}{\cos(\pi\xi) - \cos(\pi\xi')}. \quad (42)$$

Substituting expressions (13) (i.e., $E_x(\xi, 0) = J/e\mu n_s(\xi)$), (22), and (42) into (40) at $\eta = 0$, we again find a nonlinear integral equation for the dimensionless carrier concentration ν_s (defined as in (19)). For the present geometry this equation is of the form

$$\frac{1}{\nu_s(\xi)} = \int_0^1 d\xi' \left(\frac{1}{\nu_s(\xi')} - \frac{\pi\nu_s(\xi') \sin(\pi\xi')}{\cos(\pi\xi) - \cos(\pi\xi')} \right) \quad (43)$$

and a good approximation of its solution is given by

$$\nu_s(\xi) = a\xi^{\alpha}(1 - \xi)^{\beta} \quad (44)$$

with $a^2 \approx 0.22$, $\alpha \approx 0.36$, and $\beta \approx 0.1$. When substituted in (22), this yields a current–voltage characteristic of the form (2) with

$$\zeta_2^c \approx \frac{\pi a^2}{2} \frac{[\Gamma(2 - \alpha - \beta)]^2}{[\Gamma(1 - \alpha)\,\Gamma(1 - \beta)]^2} \approx 1.0. \quad (45)$$

Compared to the case of point contacts (Section III-A), in the present geometry the electron concentration decreases more slowly away from the cathode contact and toward the anode, while the current for the same bias is nearly twice larger. The case of strip contacts (Section III-B) is roughly in between these two limits.

IV. Numerical Simulation of the SCL Current in Films and Comparison to Analytic Results

To verify the correctness of our analytical description of the SCL current in thin films and to extend the treatment to the case of a finite film width D, we have performed numerical simulations of the problem, taking into account both the drift and the diffusion transport mechanisms, as well as the effects of field-dependent mobility. In these simulations, we assumed a material with relative permittivity $\epsilon = 10$ and doping concentration $N_{\text{background}} = 10^{12}$ cm^{-3} (at such low concentrations, none of the calculated characteristics was sensitive to a variation in $N_{\text{background}}$). The contacts were assumed doped to 10^{19} cm^{-3} with a Gaussian tail of length scale 0.01 μm at the junction with the low-doped material. The low-field mobility was assumed to be equal to $\mu = 10^3$ V cm/s and the diffusion coefficient was defined by the Einstein relation at $T = 300$ K. In most of the simulations the diode base length was taken to be $L = 4.8$ μm—except, of course, when the dependence on L itself was investigated.

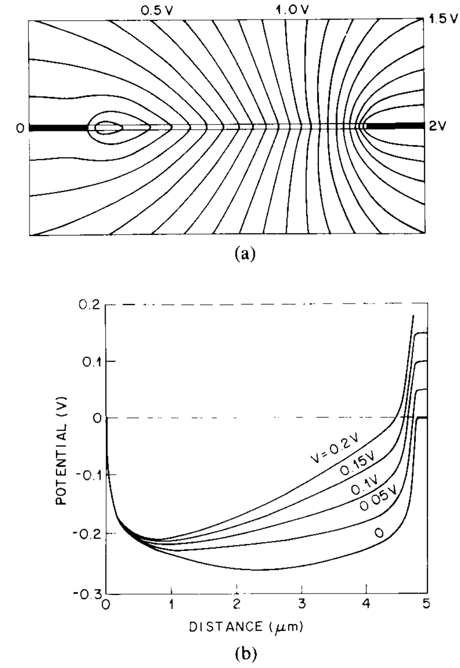

Fig. 3. Two-dimensional distribution of the electrostatic potential within and around a thin-film diode carrying current for the case of strip-contact geometry. The base length $L = 4.8$ μm and the film thickness is 0.1 μm. (a) Equipotential lines for two applied biases, $V = 2$ V ($J = 1.7 \times 10^{-6}$ A/μm) and $V = 4$ V ($J = 6 \times 10^{-6}$ A/μm). (b) Variation of the potential along the center of the film for several different bias voltages.

For thick films $D \gtrsim L$ under high bias ($\gtrsim 10kT$), the numerically calculated I–V characteristic coincides with the Mott–Gurney law (12).

Although we have performed simulations for all three contact geometries (Fig. 1(a)–(c)), for the sake of brevity only results corresponding to the *strip-contact geometry* will be presented below. These results were found to be sufficiently illustrative of the main features of the SCL current phenomenon in thin films.

Fig. 3(a) illustrates the two-dimensional distribution of the electrostatic potential within and around a thin-film diode carrying current. Equipotential lines are shown for a linear current density $J \approx 1.7 \times 10^{-6}$ A/μm. The variation of the potential along the center of the film is shown in Fig. 3(b) for several different bias voltages. It is evident that with increasing bias the virtual-cathode position moves toward the cathode.

Fig. 4 shows the current–voltage characteristics calculated using the constant-mobility approximation for different film thicknesses. We see that, as D decreases, the simulated curves converge toward our analytical result, obtained in Section III-B. The deviation at low voltages can be attributed to our neglect of diffusion; this deviation is substantially weaker in the case of edge contacts. Simulation shows that the virtual cathode approaches the cathode faster in that case. It is clear that the virtual cathode approximation leads to an underestimate of the current because it overestimates the effective diode length. When $D \lesssim 0.2$ μm, there is almost no variation of the

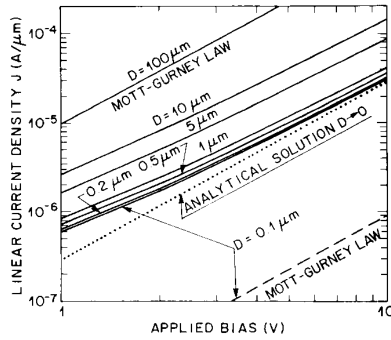

Fig. 4. Current-voltage characteristics of a thin-film diode for the case of strip-contact geometry. Solid lines show the curves calculated numerically for different film thicknesses D with a drift-diffusion simulator, assuming a constant mobility $\mu = 1000$ cm^2/Vs and an associated diffusion coefficient determined by Einstein's relationship at room temperature. The dotted line corresponds to our analytical expression, (2) and (31). Also shown are the predictions of the Mott-Gurney law for two values of D. For $D = 100$ μm, this law agrees with the numerical simulation to within the accuracy of the figure. In contrast, for a thin film, the Mott-Gurney law (dashed line) gives a current density that is lower than the actual current by more than an order of magnitude.

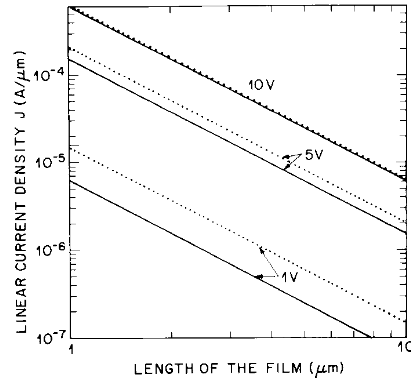

Fig. 6. Dependence of the current-voltage characteristics on the length of the film L for three bias voltages. The solid lines correspond to our analytical expressions, and the dotted curves have been calculated for $D = 0.1$ μm with the help of a drift-diffusion simulator and the physical parameters as in Fig. 4.

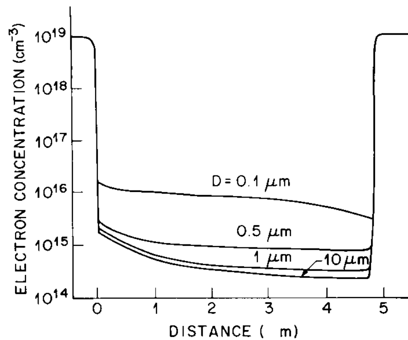

Fig. 5. Injected carrier concentration in a thin-film diode calculated with a drift-diffusion simulator assuming the same physical parameters as in Fig. 4.

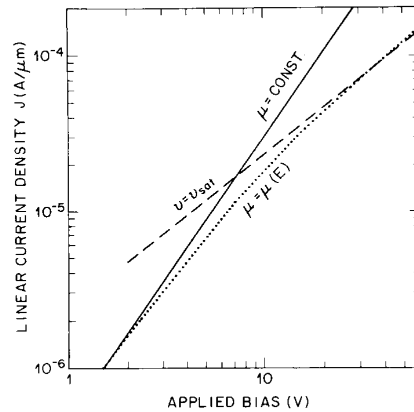

Fig. 7. Illustration of the effect of velocity saturation on the current-voltage characteristics of a thin-film diode ($L = 4.8$ μm) for the case of strip-contact geometry. Dotted line shows the results calculated for $D = 0.1$ μm by our drift-diffusion simulator, assuming a field-dependent mobility (see (46)) with the low-field value $\mu = 1000$ cm^2/Vs and $v_{sat} = 10^7$ cm/s. Solid line corresponds to a simulation in which the velocity-field characteristic was assumed in the form $v = \mu E_x$ with a constant $\mu = 1000$ cm^2/Vs. The dashed line was calculated with (34), corresponding to a constant drift velocity v_{sat}.

current with the further decrease on D, which means that the latter is entirely compensated by the increasing volume density of charge in the film, so that the surface concentration $n_s(x)$ becomes independent of D. The actual distribution of n_s in the film, calculated under conditions similar to those in Fig. 4, is shown in Fig. 5. We see from these figures that the level of injection, and consequently the current density, can be substantially higher (by an order of magnitude) in a thin-film diode than in the bulk case. Physically, this is due to the fact that the electric field lines spread out of the film, thus relaxing the space-charge limitation of carrier injection. Because of that, the dependence of SCL current on the diode *length* L differs from the bulk case. The L dependence of the simulated I-V characteristics (Fig. 6) fits the L^{-2} law, already surmised in (2) and rigorously derived in Section III.

Finally, the effect of velocity saturation is illustrated in Fig. 7. In this case the velocity-field curve assumed in our drift-diffusion simulator was of the form

$$v = \frac{\mu E_x}{\left[1 + (\mu E_x / v_{sat})^2\right]^{1/2}}. \tag{46}$$

We see that the simulated current-voltage characteristic nicely interpolates between the analytically calculated limits of constant mobility (valid when $\mu E_x \ll v_{sat}$ over most of the diode base) and constant drift velocity $v = v_{sat}$ at high applied fields.

V. Conclusion

We have considered the space-charge-limited current for an n-i-n diode in which the current flow is confined to a thin film of thickness D. Because the electric field of

injected electrons spreads out of the film, the level of injection is substantially higher than in the bulk case described by the classical Mott–Gurney law. As a consequence, the current density in a thin-film diode can be an order of magnitude larger than in a bulk diode of same length. It is shown that, in the limit of small D, the total current is independent of D because the decreasing film thickness is exactly compensated by increasing injection. In this limit, we have obtained analytic expressions of the current–voltage characteristics for three representative electrode configurations. Our theoretical analysis has been carried out for two model velocity-field relationships: that of a constant mobility and that of a constant (saturated) drift velocity. The analytic results are confirmed by a numerical simulation of the diode within a drift-diffusion model. Results of the simulation also describe a transition with decreasing D from the Mott–Gurney law to the law governing space-charge-limited current in a film.

Our method of solution employs the Green function of the Poisson equation describing the electric field of the injected charge and the charge induced on the electrodes. On extended electrodes the induced charge is distributed in a nontrivial way, and we take it into account by using a Green function, satisfying the boundary condition of a fixed potential on the conducting electrode surfaces. The total potential and field distribution in the device is found next by integrating over the injected charge density. This procedure leads to a nonlinear integral equation for the injected charge density, which we solve numerically as well as analytically, and then the SCL current–voltage characteristic is readily determined.

It should be emphasized that a similar procedure can be applied to the calculation of the field distribution and the current–voltage characteristics of a field-effect transistor. In this way one can construct analytical FET models that go beyond the usual gradual-channel approximation. The first such model was discussed by Geurst [3] on the basis of his treatment [2] of the SCL current in thin films. Although Geurst's model was very schematic, it proved useful for the elucidation of details of the current formation in short-channel devices. Our method presented here is quite different from that employed by Geurst [2]: it is physically more transparent and lends itself to extensions in a straightforward manner. This gives us grounds to believe that it will enable an analytic description of more realistic FET models.

Appendix

Numerical Solution of the Nonlinear Integral Equations for the Injected Charge Density

Considering the SCL current in thin-film diodes of three different contact geometries, corresponding to Fig. 1(a)–(c), we have reduced the problem to nonlinear integral equations (20), (29), and (43), respectively. For each of these equations we have found an approximate solution, by assuming a reasonable form of the solution, viz. (21), (30), and (44)—containing adjustable parameters—and then minimizing the error by varying these parameters. The resultant solutions have been checked against the corresponding numerical solutions of the integral equations.

The numerical procedure used consists of the following. First, the equation to be solved is rewritten so that the solution is bounded, while the principal value of the integral is done analytically. The resultant equation is solved using POST [8] with the integral done by Gaussian quadrature rules that avoid divisions by 0. The mesh needed to get the solution accurately is generated automatically by SSAF [9], a package for fitting functions defined by subroutines—such as calls to POST. This procedure is illustrated below in the instance of (20).

Since the solution of this equation is expected to be singular at $x = 0$, we solve for a bounded function

$$u(x) \equiv \int_0^x (1 - \xi)\nu_s(\xi)\, d\xi \tag{A1}$$

from which ν_s is determined by

$$\nu_s(x) \equiv \frac{u'(x)}{(1 - x)}. \tag{A2}$$

This transforms (20) into

$$u'(x) \int_0^1 \frac{u'(y)}{x - y}\, dy = (1 - x)^2. \tag{A3}$$

To reduce the singularity present in the integral of (A3), we use the relation

$$\int_0^1 \frac{dy}{y - x} = \ln\left(\frac{1 - x}{x}\right)$$

and rewrite (A3) as

$$[u'(x)]^2 \ln\left(\frac{1 - x}{x}\right) + u'(x) \int_0^1 \frac{u'(x) - u'(y)}{x - y}\, dy = -(1 - x)^2. \tag{A4}$$

The technique described in example 8 of POST [8] is used to discretize (A4). Fourth-order ($k = 4$, cubic) splines are used to solve (A4) because u' is needed accurately. To keep the programming simple, and have it vectorize on the Cray XMP, divisions by zero are avoided by replacing $\int_0^1$ by the slightly different $\int_\epsilon^{1-\epsilon}$, where ϵ is the machine rounding error, roughly 10^{-14}. To avoid divisions by 0 from $x - y$, the Gaussian quadrature rule used for the integral is chosen to be a six-point rule. Since the quadrature rule used inside POST for $k = 4$ is a four point rule, this guarantees that $x - y$ is never 0 in the discrete solution process.

For the above solution technique to work effectively, it is necessary to have a good mesh for discretizing the problem. Since the solution is expected to have singularities in its derivatives at the end-points, it is difficult to make a good mesh by hand. The mesh is automatically

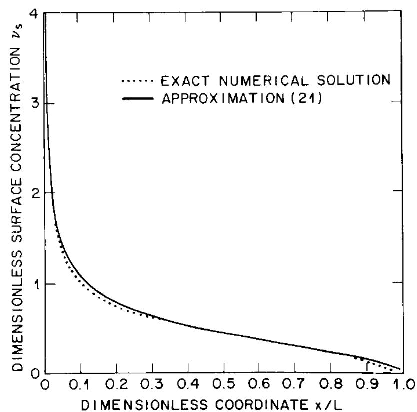

Fig. 8. Comparison of the analytic approximation (21) (solid curve) with the exact numerical solution of (20) (dotted curve).

obtained using SSAF [9]. The function to be fitted, $u(x)$, is defined for SSAF by a routine solving (A4) on the mesh specified. The mesh chosen by SSAF for graphical (1 percent) accuracy typically has 60 mesh points (for $k = 4$, cubic, splines) and the points are very densely distributed near $x = 0$, where the singularity of the derivatives is greatest.

Fig. 8 compares the resultant numerical solution of (20) for $\nu_s(x)$ with our analytical approximation (21). The agreement is seen to be excellent.

References

[1] N. F. Mott, and R. W. Gurney, *Electronic Processes in Ionic Crystals*, 2nd ed. Oxford: Oxford University Press, 1948.

[2] J. A. Geurst, *Phys. Status Solidi*, vol. 15, p. 107, 1966.

[3] —, *Solid-State Electron.*, vol. 9, p. 129, 1966.

[4] A. A. Grinberg and S. Luryi, *J. Appl. Phys.*, vol. 61, p. 1181, 1987.

[5] C. D. Child, *Phys. Rev.*, vol. 32, p. 492, 1911.

[6] B. A. Fuchs and B. V. Shabat, *Functions of Complex Variables and Some of Their Applications*, vol. 1. Oxford: Pergamon, 1964.

[7] W. R. Smythe, *Static and Dynamic Electricity*, 2nd ed. New York: McGraw-Hill, 1950.

[8] N. L. Schryer, "Partial differential equations in one space variable," Bell Labs. Computing Science Tech. Rep. 115, 1984.

[9] —, "SSAF—Smooth spline approximation to functions," AT&T Bell Labs. Computing Science Tech. Rep. 131, 1986.

*

Anatoly A. Grinberg received the Ph.D degree in 1961 from the Lebedev Institute of Physics, Moscow, U.S.S.R., and the Dr.Sci. degree in 1969 from the A. F. Ioffe Institute of Physics and Technology, Leningrad, U.S.S.R.

Until 1980, he worked at the A. F. Ioffe Institute as a Senior Staff Scientist. In 1980, he joined the Department of Physics of New York University. Since 1982, he has been associated with the Department of Electrical Engineering of the University of Minnesota, and since 1985, he also has been with AT&T Bell Laboratories where he is currently a Member of Technical Staff. His research has included transport properties as well as linear and nonlinear optics of semiconductors, properties of two-dimensional electron gas, and high-speed devices. His work has appeared in over 90 publications in physics and engineering journals.

*

Serge Luryi (M'81-SM'85-F'89) received the M.Sc. and Ph.D. degrees in theoretical physics from the University of Toronto in 1975 and 1978, respectively.

Since 1980, he has been a member of the technical staff at AT&T Bell Laboratories, Murray Hill, NJ, where he is currently a group supervisor in the Solid State Electronics Research Laboratory. His main research interests are in the physics of exploratory semiconductor devices.

*

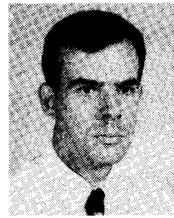

Mark R. Pinto (S'84-M'85) received the B.S. degrees in electrical engineering and computer science form Rensselaer Polytechnique Institute, Troy, NY, and the M.S. and Ph.D. degrees in electrical engineering from Stanford University, Stanford, CA.

He has held summer positions at Hughes Aircraft Company, Rockwell International, IBM Research, and AT&T Bell Laboratories, all in IC technology research. He is currently a member of the Technical Staff at AT&T Bell Laboratories, Murray Hill, NJ, where he is working on research of small-geometry devices.

Dr. Pinto is a member of Tau Beta Kappa and Eta Kappa Nu.

*

Norman L. Schryer received the Ph.D. degree in mathematics from the University of Michigan in 1969.

After graduating, he joined the Computing Science Research Center of AT&T Bell Laboratories. His main interest is in the numerical solution of partial differential equations.

Dr. Schryer is a member of the American Mathematical Society, the Association for Computing Machinery, and the Society for Industrial and Applied Mathematics.